Appl. Phys. A (2017) 123:357
DOI 10.1007/s00339-017-0963-9

Applied Physics A
Materials Science & Processing

Ag–TiO_2 composite photoelectrode for dye-sensitized solar cell

Wan-Yu Wu[1] · Chun-Fa Hsu[2] · Menq-Jion Wu[2] · Chao-Nan Chen[3] · Jung-Jie Huang[4]

Received: 25 January 2017 / Accepted: 7 April 2017 / Published online: 18 April 2017

Abstract In this study, Ag nanoparticles were introduced into the titanium oxide (TiO_2) photoelectrode to fabricate dye-sensitized solar cells (DSSCs). The Ag nanoparticles were synthesized using a chemical reduction method. By varying the concentration of the reducing agent ($NaBH_4$), Ag nanoparticles with different sizes were obtained and discussed. The Ag–TiO_2 composite photoelectrode was fabricated using a simple approach by immersing sintered P-25 photoelectrode into the solution containing Ag nanoparticles. The DSSC using Ag–TiO_2 composite photoelectrode exhibits better solar conversion efficiency than that using simply TiO_2 photoelectrode (P-25). The DSSC efficiency enhances from 2.75 to 5.66% using larger Ag nanoparticle size of 82.7 nm.

1 Introduction

Dye-sensitized solar cell (DSSC), one of the third generation solar cells, has attracted great attention and has been extensively studied due to their relatively high efficiency (~13%), low-cost process, and high potential for roll-to-roll manufacture [1–4]. Therefore, DSSCs have emerged to be one of the most promising alternatives to conventional silicon-based solar cells [5–8]. Although DSSCs have been industrially fabricated with cell efficiency around 8%, researches for further improving the efficiency are still on demand [9]. Therefore, investigations on photoelectrodes [10, 11], electrolyte [2, 12], and counter electrode [5–8, 13] have been performed to improve electron transport, reduce electron–hole recombination, and increase light harvesting efficiency of the DSSCs. Approaches such as increasing the optical absorption by introducing metallic nanoparticles into TiO_2 electrode [14–16], using an oxide barrier layer (ZnO, TiO_2, etc.) to reduce the recombination of electron in the dye or electrolyte [17, 18], and lengthening the optical path within TiO_2 electrode by introducing a scattering layer [19, 20] have been taken. Among these approaches, adding metallic nanoparticles into TiO_2 photoelectrode can enhance the optical absorption by inducing localized surface plasmas [21]. Furthermore, metallic nanoparticles lead to the formation of Schottky barriers at metal-TiO_2 interfaces for reducing the electron recombination [22], reflect and scatter incident light for lengthening the optical path in electrodes [23], and forms an electron transfer network [24]. Ag and Au nanoparticles with sizes from 10 to 100 nm are the most studied in for such purposes [21, 25–27]. The techniques for preparing Au– or Ag–TiO_2 photoelectrode include physically mixing metal and TiO_2 [15, 16, 22, 26, 27] and immersing TiO_2 electrode into a dispersion solution containing Au nanoparticles [21] or into $AgNO_3$ solution then reduce the Ag ions by traditional method (UV light), such as thermal evaporation and atomic laser deposition have also been used to deposited Ag islands or layers [25]. Traditional method techniques are inexpensive and simple. However, the reaction process need to spend long time and it will be easier for the aggregation of nanoparticle. Chemical

✉ Jung-Jie Huang
jjhuang@mail.dyu.edu.tw

[1] Department of Materials Science and Engineering, Da-Yeh University, Changhua 51591, Taiwan

[2] Department of Mechatronics Engineering, National Changhua University of Education, Changhua 500, Taiwan

[3] Department of Computer Science and Information Engineering, Asia University, Taichung 41354, Taiwan

[4] Department of Electrical Engineering, Da-Yeh University, Changhua 51591, Taiwan

reduction methods have been extensively used in the preparation of nanoparticles that has advantages such as carried out at room temperature, simplicity, low-coat process and suitability for mass production [28].

Although the multiple advantages including plasmon-enhanced optical absorption, enhanced light diffuse reflection, and reduced recombination rate have been reported for adding Ag nanoparticles into TiO_2 photoelectrode, the characteristics of Ag nanoparticles in TiO_2 photoelectrode remain required. In this study, the Ag nanoparticles were synthesized using a chemical reduction method in which the concentration of the reducing agent ($NaBH_4$) was varied. Ag nanoparticles synthesized using different reducing agent ranging from 1×10^{-4} to 5×10^{-3} M leads to different nanoparticles sizes and distribution. The Ag–TiO_2 composite photoelectrode was fabricated using a simple approach by immersing sintered P-25 photoelectrode into the Ag nanoparticle dispersion solution. The porous TiO_2 photoelectrode allows Ag nanoparticles to penetrate into and distribute randomly within the photoelectrode. The characteristics of Ag–TiO_2 composite photoelectrode and the depth-profiled concentration of Ag and the TiO_2 surface bonding were reported in this paper.

2 Experimental

2.1 Silver nanoparticles synthesis

For synthesizing silver nanoparticles, 30 ml of silver nitrate solution with a concentration of 0.1 M was first prepared by adding Silver nitrate ($AgNO_3$, 99.8%, Showa) into de-ionized (DI) water. Sodium salt of polynaphthalene sulfonate formaldehyde condensate (Daxad19, 98%, Gelest) was used as a surfactant. Then, 10-ml solution of in DI water with 10^{-3} M Daxad19 was added into the silver nitrate solution. After 5 min of stirring, 5 ml of reducing agent, sodium tetrahydridoborate ($NaBH_4$, 98%, Aldrich) was added with a fixed speed of 1 mL/min. The concentration of $NaBH_4$ was varied from 1×10^{-4} to 5×10^{-3} M. After 30 min of stirring, the color of the solution became yellow or black depending on the concentration of reducing agent which indicate that silver nanoparticles were formed.

2.2 TiO_2 and Ag–TiO_2 photoelectrode fabrication

TiO_2 paste was prepared by adding 2 g of TiO_2 powder (P25, 99.9%, Degussa) into 7 mL of ethanol (99.5%, Aldrich). After 30 min of stirring, 0.7 mL of acetyl acetone (99%, Aldrich) and 0.1 mL of triton X-100 (99%, Aldrich) were sequentially poured into the TiO_2 solution and stirred for another 24 h for preparing the TiO_2 paste. A two-step spin-coating process (700 rpm for 20 s and 1500 rpm for 20 s) was used to coat the TiO_2 paste on indium-tin-oxide (ITO) conducting glass substrate (Rui Long Optical, Taiwan, 2.8 mm thickness, 8 Ω/sq), and the defined active area of the photoelectrode was 0.16 cm^2. After drying at 60 °C for 10 min, the resulting coating was sintered at 450 °C for 1 h with a heating rate of 5 °C/min in an ambient environment to obtain TiO_2 photoelectrode. The Ag–TiO_2 composite photoelectrode was prepared by immersing the sintered-TiO_2 photoelectrode into the 5-mL Ag dispersion solution for 10 min. Then the Ag–TiO_2 composite photoelectrode was sintered at 250 °C for 30 min in an ambient environment.

2.3 DSSCs assembly

The resulting TiO_2 and Ag–TiO_2 photoelectrodes with a thickness of approximately 7 μm were immersed in a 0.5 mM of N719 dye (Solaronix SA) for 18 h. After the dye adsorption, the TiO_2 and Ag–TiO_2 photoelectrodes were rinsed with ethanol to remove the excess dye and dried with a nitrogen stream. The electrolyte was acetonitrile consisting of 0.1 M LiI (99%, Aldrich), 0.6 M 1, 2-dimethyl-3-propylimidazolium iodide, 0.05 M I_2 (99.8%, Aldrich) and 1.0 M 4-*tert*-butylpyridine (96%, Aldrich). The Pt counter electrode was prepared by sputtering a Pt layer with a thickness around 60 nm on the ITO glass.

2.4 Characterization and measurements

The absorption spectra of the Ag dispersion solution were measured using an ultraviolet/visible/near infrared (UV–Vis-NIR) spectrophotometer (JASCO, V570). The particle size and their distribution was analyzed using particle size analyzer (SHIMADAZU IG-1000 plus). After the coating and sinter process, the crystalline phases of TiO_2 and Ag–TiO_2 photoelectrodes were characterized using grazing incident X-ray diffractometer (GIXRD; PANalytical, X'Pert Pro MRD) with an incident angle of 1° and a scanning speed of 1.2°/min. The TiO_2 and Ag–TiO_2 photoelectrodes surface morphology were examined using field emission scanning electron microscopy (FE-SEM; JEOL, JSM-7000F). Auger electron spectroscopy (JEOL-JAMP-9500F) was used to examine the depth-profiled concentration of Ag. Additionally, the depth profile and the chemical bonding state of the TiO_2 and Ag–TiO_2 photoelectrodes were analyzed using X-ray photoelectron spectroscopy (XPS; ULVAC, PHI 5000). The current–voltage (*J*–*V*) curves of the DSSCs were measured by a Keithley digital source meter (Model 2400) under an AAA solar simulator with AM 1.5 sunlight at 100 mW/cm^2 [10].

3 Results and discussion

Figure 1 shows the UV–V absorption spectra of Ag dispersion solution is synthesized using various reducing agent concentrations. The absorption band around 410–430 nm is seen [29]. It was also observed that the intensity of the absorption peak increases with the reducing agent concentration. The insert photo in Fig. 1 shows the color of the Ag nanoparticle dispersion solution changing from light yellow to dark brown with increasing reducing agent concentration.

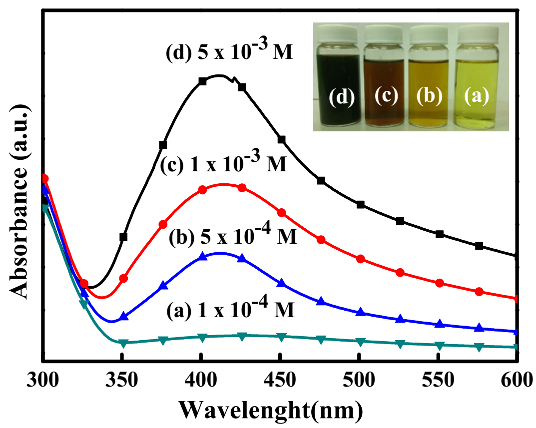

Fig. 1 UV–V is absorption spectra of Ag nanoparticles synthesized using various reducing agent concentrations

Figure 2 shows the size distribution profile of the Ag in the dispersive solution measured by particle size analyzer. Data analysis using the cumulant method was achieved and the results were listed in the individual figures. It was found that the diameter of the Ag nanoparticle in Fig. 2 is consistent with that measured by the SEM. An increased Ag size and a higher polydispersity index (PI) were observed as increasing the concentration of reducing agent. A small value of PI gives uniform (monodisperse) dispersion. A high concentration of the reducing agent leads to a fast reduction rate of Ag ions. The nucleation and also the growth of Ag nanoparticles were, therefore, enhanced. As a result, the dispersive solution reduced using 5×10^{-3} M reducing agent that has large Ag nanoparticles and a non-uniform dispersity. The color of the Ag dispersion solution, therefore, becomes darker. In addition, the divided peaks indicated that the aggregation phenomenon occurred as the reducing agent concentration at 5×10^{-3} M. In addition, the pH value of the Ag dispersion solution varied from 5.3 to 3.7 as increasing the reducing agent concentration. Except the fast nucleation and growth of Ag, the acid environment also plays a role in the aggregation phenomenon.

After the photoelectrode fabrication and the DSSCs assembly process, the performance of DSSCs was analyzed. Figure 3a shows the J–V curves of DSSCs using TiO_2 and Ag–TiO_2 as the photoelectrode. The insert table indicates the short current density (J_{sc}), open circuit voltage (V_{oc}), fill factor (FF), and solar conversion

Fig. 2 The size distribution profile of the Ag in the dispersive solution measured by particle size analyzer under various reducing agent concentrations

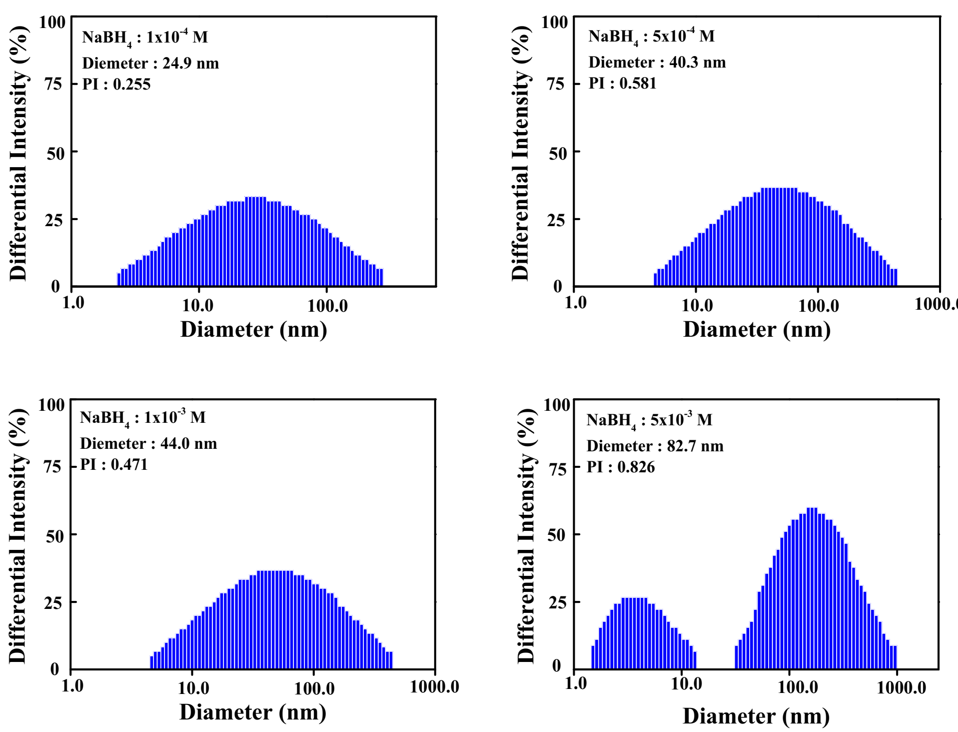

efficiency (η) of the DSSCs. It shows that the efficiency is enhanced using the Ag–TiO_2 composite photoelectrode. Moreover, a large size and a high PI value of Ag nanoparticles give a higher efficiency. The enhanced J_{sc} from 7.21 to 12.29 mA/cm^2 and solar conversion efficiency from 3.40 to 5.66% is apparent. Compared to the cell efficiency of TiO_2 photoelectrode without adding Ag nanoparticles, the highest enhancement of 106% was achieved using the Ag–TiO_2 photoelectrode having Ag nanoparticle size of 82.7 nm. The explanation of the enhanced cell efficiency will be addressed later. The Ag nanoparticles in Fig. 3b were synthesized using different reducing agent concentrations, as mentioned above, to have various Ag nanoparticle size. In the wavelengths from 400 to 800 nm, the absorbance is apparently enhanced with the reducing agent concentration, as shown in Fig. 3b. It is known that metal particles absorb light more efficiently than most of the dyes. As the Ag nanoparticle size increases, the surface plasmon of the Ag nanoparticles leads to an enhanced light absorption of the dye. Therefore, a light scattering leading to prolonged length of light-path also contributes to the enhanced light absorption and reduced transmittance.

To understand the effect of using Ag–TiO_2 composite photoelectrode in DSSC, the characteristic of the Ag–TiO_2 photoelectrode having the highest efficiency was also made in this study. Figure 4 shows the XRD patterns of pure TiO_2 and Ag–TiO_2 photoelectrodes. Diffraction peaks located at $2\theta = 25.28°$, 37.8°, 48.05°, 53.89°, 62.96° and 75.03° are assigned to the (101), (004), (200), (105), (204) and (215) lattice planes of TiO_2, which are the anatase phase. Minor rutile phase was obtained. Both anatase and rutile phase are from the P-25 commercial TiO_2 nanoparticles. The Ag nanoparticle peak located at $2\theta = 38.75°$, 44.13°, 64.74° and 78.30° are assigned to the FCC structure containing (111), (200), (202) and (311) plane.

In the Fig. 3a show the *J*–*V* curves of DSSCs using TiO_2 and Ag–TiO_2 as the photoelectrode. The highest conversion efficiency was using the Ag–TiO_2 photoelectrode with the Ag nanoparticle size of 82.7 nm. To observe the distribution of silver nanoparticle on the surface of TiO_2 photoelectrode, the various magnification of SEM image was performed. Figure 5a–c show the surface morphologies of the bare TiO_2 and Ag (82.7 nm)–TiO_2 photoelectrodes. Figure 5a is the surface morphology of TiO_2 without immersing into the Ag solution. The cracks occur after the sintering process. After immersing the TiO_2 photoelectrode into the Ag dispersive solution, the Ag–TiO_2 composite photoelectrode was sintered at 250 °C for 30 min in an ambient environment. Figure 5b shows the surface of Ag (82.7 nm)–TiO_2 composite photoelectrode. At a higher magnification as shown in Fig. 5c, it was observed that the bright spots with various sizes are the clusters of Ag nanoparticles. Comparing Fig. 5b with a, the surface become rough after introducing Ag into the TiO_2 photoelectrode. As seen in Fig. 5c, it is noted that the Ag (82.7 nm)–TiO_2 photoelectrodes are still porous which is

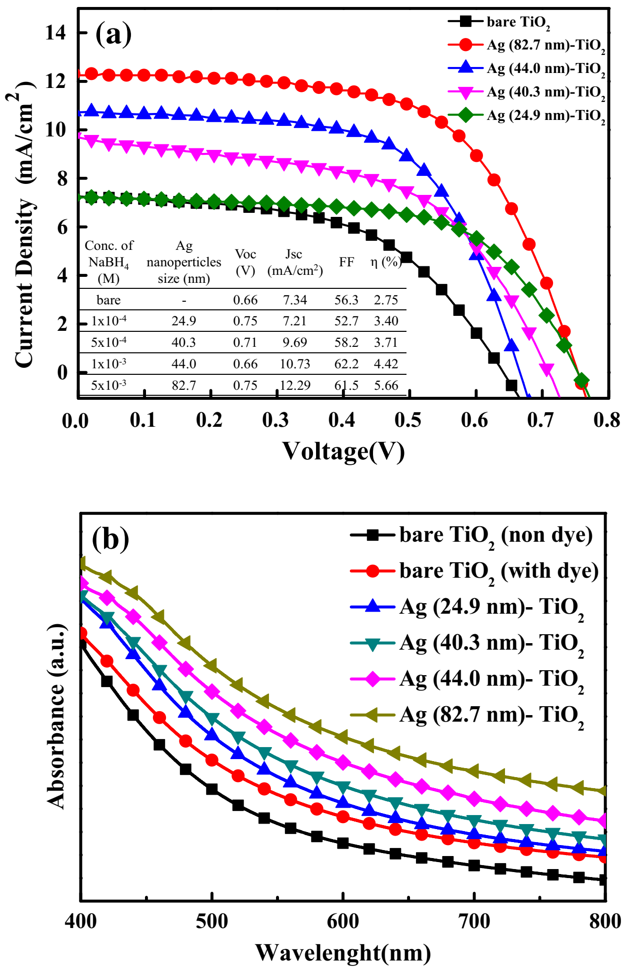

Fig. 3 *J*–*V* curves of DSSCs using TiO_2 and Ag–TiO_2 photoelectrode with different Ag nanoparticle sizes

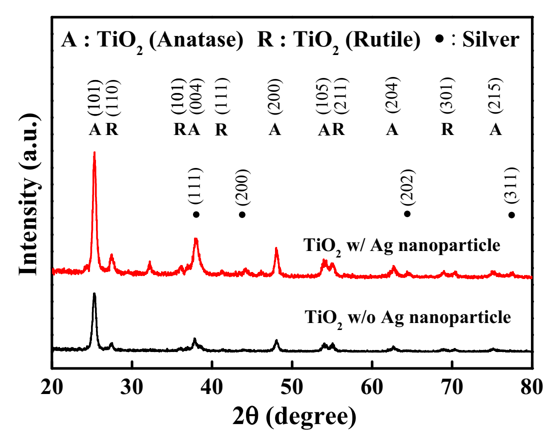

Fig. 4 X-ray diffraction (XRD) spectra of TiO_2 and Ag–TiO_2 photoelectrode

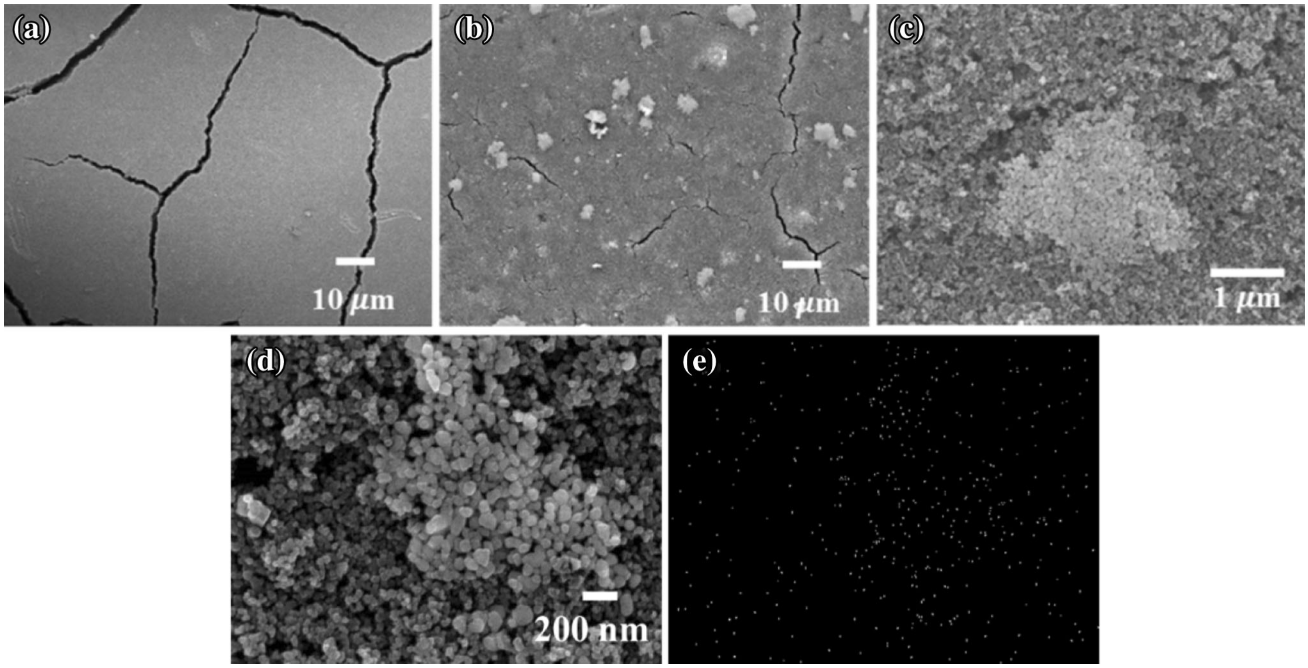

Fig. 5 SEM images of Ag (82.7 nm)–TiO_2 photoelectrode under different magnification **a** bare TiO_2 photoelectrode at ×1000 magnification; **b** ×1000; **c** ×10,000; **d** ×50,000 and **e** EDS mapping of Ag (82.7 nm)–TiO_2 photoelectrode

important for dye absorption. Figure 5d, e have been added in the manuscript. Figure 5d shows the high-magnification image of the white cluster in the Fig. 5b. Figure 5e shows the EDS elemental mapping of the Fig. 5d. From Fig. 5d, e, it is clear observed that the Ag nanoparticles aggregate into Ag cluster and distributing on the surface of the TiO_2 photoelectrode. Furthermore, the dispersive Ag nanoparticles are also observed around the Ag cluster. Besides, it was believed that the aggregated Ag cluster on the TiO_2 photoelectrode act as a scattering center to reflect the incident light backward to the photoelectrode. The photocurrent was, therefore, increased by lengthening the optical path within TiO_2 electrode.

The depth profile and the quantitative analyses of the TiO_2 and 82.7-nm Ag–TiO_2 photoelectrode obtained after the dye absorption was analyzed by XPS and AES as shown in Fig. 6. Figure 6a, b show the XPS depth profile for TiO_2 and Ag–TiO_2, respectively. The measured depth is around 120 nm from the surface. The signals of C and Ru are from the dye while Ti and O are from P-25 TiO_2. In Fig. 6b, the minor S signal is from the surfactant Daxad19. The Ag signal shows stable concentration of 8 at.% within the coating surface of photoelectrodes. Such result indicates that the Ag nanoparticles passed the porous TiO_2 and distributed unformly within the porous TiO_2 layer. The results of the AES depth profile (500 nm from the surface) as shown in Fig. 6c also confirm the result we have observed in Fig. 6b. It was, therefore, believed that the Ag nanoparticles have a size smaller than the porous TiO_2 pores diffuse toward the photoelectrode. The aggregated Ag nanoparticles with large size remain on the surface of the photoelectrode. Therefore, it is believed that the surface and well distributed Ag nanoparticles lead to a reduced series resistance and an enhanced scattering effect of the incident light in the Ag–TiO_2 photoelectrode. Furthermore, as shown in Fig. 6a, b, the C signal originated from the dye decays rapidly within the 20 nm of surface while the minor Ru signal remain constant. However, it was found that the C signal in Ag–TiO_2 photoelectrode is 10 at.% more than that in TiO_2 photoelectrodes. The C signal decay to almost zero at.% within the 120 nm of surface for TiO_2 photoelectrode while it decays to 10 at.% and become steady for Ag–TiO_2 composite photoelectrode. Such results indicate that the dye absorption was enhanced after adding Ag into TiO_2 photoelectrode. As mentioned above, the pH value of Ag dispersive solution is more acid as the reducing agent concentration at 5×10^{-3} M. Moreover, the dye attachment occurs through the anchoring between the COOH of dye and the –OH on TiO_2 surface [30–32]. As a result, dye absorption was, therefore, enhanced by introducing the –OH on TiO_2 surface through the process of adding Ag nanoparticles.

The high-resolution XPS results of TiO_2 with and without dye and Ag–TiO_2 with dye were shown in Fig. 7. Figure 7a–d are the detail spectra of C1s, Ti 2p, O 1s, and Ag 3d, respectively. The C1s, as shown in Fig. 7a, shows the peaks at 284.6 and 288.1 eV are attributed to the bonding of C–C and COOH, receptively. After the dye loading, most C–C bond is contributed from the dye molecular. It was observed the C–C peak shift to a lower binding energy as Ag was introduced into the TiO_2. Such shift indicates the electronic screening of C–C bond was increased after the process of adding Ag. The Ti 2p, as shown in Fig. 7b, shows the Ti 2p3/2 and Ti 2p1/2 peaks located at 458.0 and 463.3 eV, respectively [33]. A minor chemical shift to higher binding energy was observed for both TiO_2 and Ag–TiO_2 photoelectrode w/dye. As shown in Fig. 7c, for TiO_2 w/o dye, the peaks at 529.0 and 529.7 eV are attributed to the bonding of Ti–O in TiO_2 and O–H on the TiO_2 surface, receptively [34, 35]. After dye absorption, the Ti–O peak shifts to higher binding energy for photoelectrode of TiO_2 and Ag–TiO_2. The shifting of Ti 2p and O1s for TiO_2 and Ag–TiO_2 photoelectrode results from the presence of dye based on its chemical environment. For the Ag 3d spectrum of Ag–TiO_2 with dye, Fig. 7d shows the peaks of Ag 3d5/2 and Ag 3d3/2 located at 367.1 and 373.1 eV, respectively. After peak deconvolution, peaks at 367.3 and 373.5 eV were assigned to Ag^0 while peaks at 366.9 and 373.0 eV were assigned to Ag^+ [29, 34]. Both metallic and oxidized Ag exists in Ag–TiO_2 composite photoelectrode.

According to the Ti 2p peak deconvolution, the amount of Ti^{3+} and Ti^{2+} on the Ag–TiO_2 photoelectrode surface is 41.2% higher than that on the TiO_2 photoelectrode surface. Such results also indicate that the oxygen vacancies increase and more dye absorb on the TiO_2 surface after the process of introducing Ag into TiO_2 photoelectrode [36]. As mentioned above, the dye absorption was also enhanced by introducing the –OH on TiO_2 surface through the process of adding Ag nanoparticles. Oxygen vacancies and –OH on TiO_2 surface both give a higher dye absorption and J_{sc} value.

Figure 2 shows the silver nanoparticle size was log-normal distribution. Therefore, the silver nanoparticle distribution includes various particle sizes. The XPS/AES for depth profile can prove that the Ag nanoparticles have a size smaller than the porous TiO_2 pores diffuse towards the photoelectrode. The small size of the Ag nanoparticle role might localize surface plasmas, formation of Schottky barriers at Ag–TiO_2 interfaces, and the lengthened optical path by scattering. The large size of the Ag nanoparticle was aggregated on the TiO_2 surface photoelectrode which can further enhance the photocurrent by acting as a scattering center to reflect the incident light backward to the TiO_2 photoelectrode. Additionally, it was also observed that the acid treatment by immersing the TiO_2 electrode into the Ag dispersive solution can increase the dye absorption and also enhance the photocurrent [37]. As to V_{oc}, the open circuit potential of DSSC is directly related to the concentration of electrons in the conduction band. It was believed that the Ag nanoparticle could act as active

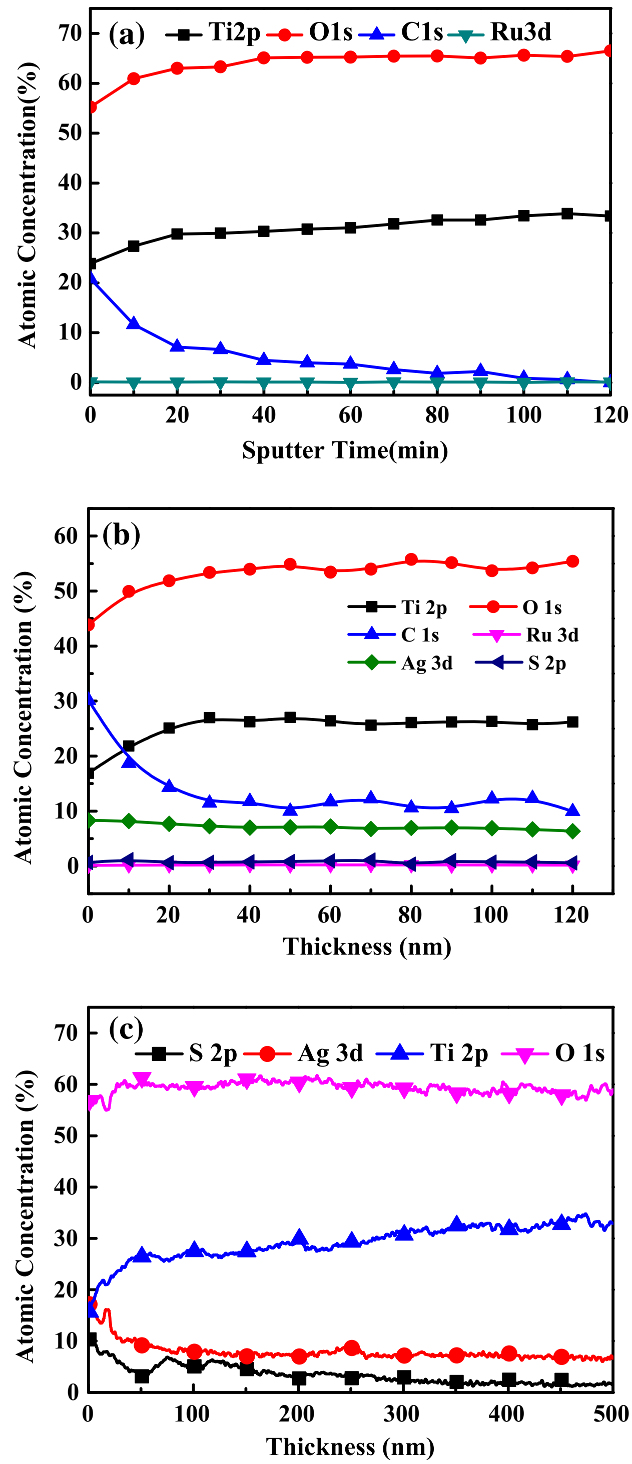

Fig. 6 The XPS depth profile of the **a** TiO_2 and **b** Ag–TiO_2 photoelectrodes. **c** The AES depth profile of the Ag–TiO_2 photoelectrode

sites to inhibit the fast recombination of electron-hole pairs. Therefore, it could effectively suppress the recombination between I_3^- and electrons transferred backward from the TiO_2 films to the electrolyte, and would make a

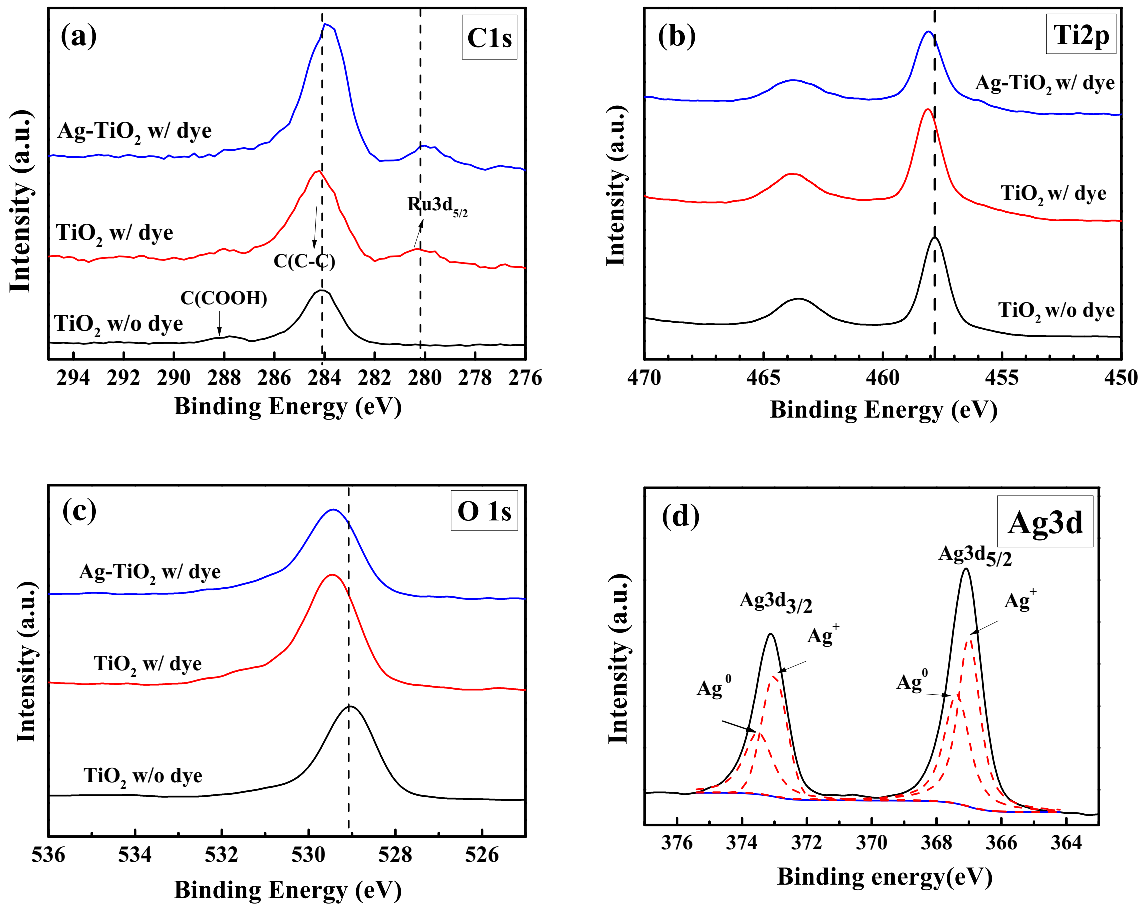

Fig. 7 XPS detail spectra of **a** C1s, **b** Ti2p, **c** O1s, and **d** Ag 3d of the TiO_2 and Ag–TiO_2 photoelectrodes

contribution to increase the V_{oc} of DSSCs [38]. Therefore, the highest cell efficiency is attributed to the interplay among the present of Ag in TiO_2 photoelectrode and the acid treatment while introducing Ag into TiO_2 photoelectrode.

4 Conclusions

In this study, the Ag nanoparticles were synthesized using a chemical reduction method in which the concentration of the reducing agent ($NaBH_4$) was varied. Dispersive Ag nanoparticles having average sizes ranging from 25 to 83 nm were obtained. The Ag–TiO_2 photoelectrode was fabricated using a simple approach by immersing sintered P-25 photoelectrode into the Ag nanoparticle dispersion solution. The DSSC efficiency was further enhanced from 3.4 to 5.66% using larger Ag nanoparticle size of 83 nm. Therefore, comparing to TiO_2 photoelectrode, the highest enhancement of 106% in efficiency was achieved using Ag–TiO_2 composite photoelectrode. In this paper, we focus on the characteristics of Ag–TiO_2 composite photoelectrode and the depth-profiled concentration of Ag and the TiO_2 surface bonding. It was found that not only the dispersive Ag nanoparticles enhance the cell performance, the aggregated Ag clusters on the surface of the TiO_2 photoelectrode can further enhance the photocurrent by acting as a scattering center to reflect the incident light. Meanwhile, the acid treatment by immersing the TiO_2 electrode into the Ag dispersive solution was found can increase the dye absorption and also enhance the photocurrent.

Acknowledgements The authors thank the Ministry of Science and Technology of the Republic of China, Taiwan, for financially supporting this research under Contract No. 105-2221-E-212-003.

References

1. B. Oregan, M. Gratzel, Nature **353**, 737 (1991)
2. S. Mathew, A. Yella, P. Gao, R. Humphry-Baker, B.F.E. Curchod, N. Ashari-Astani, I. Tavernelli, U. Rothlisberger, MdK Nazeeruddin, M. Gratzel, Nature **6**, 242 (2014)
3. M.G. Kang, N.G. Park, K.S. Ryu, S.H. Chang, K.J. Kim, Sol. Energy Mater. Sol. Cells **90**, 574 (2006)
4. S. Ito, N.L.C. Ha, G. Rothenberger, P. Liska, P. Comte, S.M. Zakeeruddin, P. Pechy, M.K. Nazeeruddin, M. Gratzel, Chem. Commun. **38**, 4004 (2006)
5. A. Hagfeldt, M. Gratzel, Acc. Chem. Res. **33**, 269 (2000)

6. C.Y. Chen, M.K. Wang, J.Y. Li, N. Pootrakulchote, L. Alibabaei, C.H. Ngoc-le, J.D. Decoppet, J.H. Tsai, C. Gratzel, C.G. Wu, S.M. Zakeeruddin, M. Gratzel, ACS Nano **3**, 3103 (2009)
7. T. Bessho, S.M. Zakeeruddin, C.Y. Yeh, W.G.E. Diau, M. Gratzel, Angew. Chem. Int. Edit. **49**, 6646 (2010)
8. M. Gratzel, Nature **414**, 338 (2001)
9. L. Han, A. Fukui, Y. Chiba, A. Islam, R. Komiya, N. Fuke, N. Koide, R. Yamanaka, M. Shimizu, Appl. Phys. Lett. **94**, 1 (2009)
10. C.H. Chao, C.L. Chang, C.H. Chan, S.Y. Lien, K.W. Weng, K.S. Yao, Thin Solid Films **518**, 7209 (2010)
11. L. Sun, S. Zhang, X. Sun, X. He, J. Nanosci. Nanotechnol. **10**, 4551 (2010)
12. P. Wang, S.M. Zakeeruddin, I. Exnar, M. Gratzel, Chem. Commun. **24**, 2972 (2002)
13. R. Mayhew, J.D. Bozym, C. Punckt, I.A. Aksay, ACS Nano **4**, 6203 (2010)
14. C. Nahm, H. Choi, J. Kim, D.R. Jung, C. Kim, J. Moon, B. Lee, B. Park, Appl. Phys. Lett. **99**, 2531071 (2011)
15. M. Ihara, M. Kanno, S. Inoue, Physica E **42**, 2867 (2010)
16. M.D. Brown, T. Suteewong, R.S.S. Kumar, V. D'Innocenzo, A. Peterozza, M.M. Lee, U. Wiesner, H.J. Snaith, Nano Lett. **11**, 438 (2011)
17. N. Huang, Y. Liu, T. Peng, X. Sun, B. Sebo, Q. Tai, H. Hu, B. Chen, S.S. Guo, X. Zhao, J. Power Sources **204**, 257 (2012)
18. M.H. Abdullah, M. Rusop, Appl. Surf. Sci. **284**, 278 (2013)
19. G.W. Adhyaksa, S.W. Baek, G.I. Lee, D.K. Lee, J.Y. Lee, J.K. Kang, Chem. Sus. Chem. **7**, 2641 (2014)
20. B. Marko, O.K. Ursa, T. Marko, J. Nanomater. **2014**, 1 (2014)
21. K.G. Deepa, P. Lekha, S. Sindhu, Sol. Energy **86**, 326 (2012)
22. C.S. Chou, R.Y. Yang, C.K. Yeh, Y.J. Lin, Power Technol **194**, 95 (2009)
23. W. Peng, Y. Zeng, H. Gong, Y.Q. Leng, Y.H. Yan, W. Hu, Solid State Electron. **89**, 116 (2013)
24. J. Li, X. Chen, N. Ai, J. Hao, Q. Chen, S. Strauf, Y. Shi, Chem. Phys. Lett. **514**, 141 (2011)
25. S.D. Standridge, G.C. Schatz, J.T. Hupp, J. Am. Chem. Soc. **131**, 8407 (2009)
26. C. Nahm, H. Choi, J. Kim, D.R. Jung, C. Kim, J. Moon, B. Lee, B. Park, Appl. Phys. Lett. **99**, 2531071 (2011)
27. S. Chang, Q. Li, X. Xiao, K.Y. Wong, T. Chen, Energy Environ. Sci. **5**, 9444 (2012)
28. Z. Zhang, L. Xu, H. Li, J. Kong, RSC Adv. **3**, 59 (2013)
29. S. Agnihotri, S. Mukherji, RSC Adv. **4**, 3974 (2014)
30. I. Jang, K. Song, J.H. Park, S.G. Oh, Bull. Korean Chem. Soc. **34**, 2883 (2013)
31. J.M. Ting, T.W. Shih, J.M. Chen, J. Electrochem. Soc. **159**, H711 (2012)
32. D. Jiang, Y. Xu, D. Wu, Y. Sun, J. Solid State Chem. **181**, 593 (2008)
33. L. Wang, L. Jia, Q. Li, Mater. Lett. **123**, 83 (2014)
34. Z. Han, J. Zhang, Y. Yu, W. Cao, Mater. Lett. **70**, 193 (2012)
35. H.X. Guo, K.L. Lin, Z.S. Zheng, F.B. Xiao, S.X. Li, Dyes Pigments **92**, 1278 (2012)
36. K.H. Park, E.M. Jin, H.B. Gu, S.E. Shim, C.K. Hong, Mater. Lett. **63**, 2208 (2009)
37. G. Kawamura, H. Ohmi, W.K. Tan, Z. Lockman, H. Muto, A. Matsuda, Nanoscale Res. Lett. **10**, 219 (2015)
38. L. Zhao, C. Zhong, Y. Wang, S. Wang, B. Dong, L. Wan, J. Power Sources **292**, 49 (2015)